Journal of Catalysis **195,** 140–150 (2000)
doi:10.1006/jcat.2000.2970, available online at http://www.idealibrary.com on IDEAL®

Support Effects on de-NO_x Catalytic Properties of Supported Tin Oxides

Aline Auroux,*,[1] Dan Sprinceana,*,†,[2] and Antonella Gervasini‡

*Institut de Recherches sur la Catalyse, CNRS, 2, av. A. Einstein, F-69626 Villeurbanne, France; †Institute of Physical Chemistry "I.G. Murgulescu," Spl. independentei 202, 77208 Bucharest, Romania; and ‡Dipartimento di Chimica Fisica ed Elettrochimica, Università di Milano, via C. Golgi 19, I-20133 Milano, Italy

Received March 23, 2000; revised June 15, 2000; accepted June 18, 2000

The influence of the carrier (i.e., SiO_2, ZrO_2, TiO_2, γ-Al_2O_3, and MgO) on the reduction pattern, the acid–base properties, and the catalytic activity of supported tin dioxide catalysts has been investigated by temperature-programmed reduction/oxidation, adsorption calorimetry, and reduction of NO_x by ethene in an oxygen-rich atmosphere. Two series of SnO_2 catalysts of low (∼3 wt%) and high (∼20 wt%) Sn content were prepared by impregnation. The dramatic influence of the support on the activity and selectivity of the SnO_2 surfaces in the NO reduction by C_2H_4 was evidenced. For the 3 wt% Sn series, 39, 38, 29, 24, and 0% conversions of 5000 ppm NO to N_2 in the presence of 90,000 ppm of O_2 at a space velocity of 50,000 h^{-1} were observed at 500°C on ZrO_2, Al_2O_3, TiO_2, SiO_2, and MgO supports, respectively. The most active catalysts at low Sn loading were those based on ZrO_2 and Al_2O_3. The integral N_2 formation rates per mole of SnO_2 ranged from 2 to 5 × 10^{-3} s^{-1} in the 350–500°C temperature domain. An increase of the Sn loading led to small positive or negative effects on the extent of the NO reduction depending on the support. A direct relationship between reducibility and catalytic activity has also been observed. Above monolayer coverage, the molecular structures of SnO_2 play an important role. For the 20 Sn wt% series, the reducibility scale for $Sn^{IV} \rightarrow Sn^{II}$, based on the temperature at the maximum of the reduction peak, is in the order SnSi-20 > SnTi-20 > SnAl-20 > SnZr-20, while the competitiveness factor increases in the same order. Finally, it appears that a relatively strong acidity is necessary for good catalytic performance, but no direct correlation between the number of acid sites and the catalytic activity was observed.

Key Words: **tin dioxide; supports; NO reduction; acidity; reducibility.**

I. INTRODUCTION

The development of catalytic methods to remove nitrogen oxides in exhaust gases with oxidizing atmospheres is an increasingly important problem. For this purpose, selective reduction of NO_x by hydrocarbons over Cu–ZSM-5 and related metal ion-exchanged zeolite catalysts has attracted considerable attention.

While zeolites are characterized by high activity but low stability in humid air, some metal oxide catalysts have also been reported to show high selectivity or durability (1). Moreover, metal oxides such as alumina, zirconia, and titania also catalyze selective NO_x reduction by hydrocarbons quite selectively in the presence of high concentrations of oxygen (2, 3). This suggests that solid acidity or basicity may be a factor controlling catalytic activity.

The system formed by SnO_2 deposited on SiO_2 or Al_2O_3 is of great interest because of the use of SnO_2 as gas sensor and conductive coating (4). Moreover, there is a great interest in SnO_2-based catalysts because of their wide range of applications in promoting various reactions, e.g., oxidative dehydrogenation reactions (5–7) and more recently the selective reduction of NO by hydrocarbons (8–11) or by methanol (12) in an oxidizing atmosphere.

Teraoka *et al.* (11) have reported that SnO_2 shows good activity for NO reduction by hydrocarbons such as CH_4, C_2H_4, and C_3H_6 in the presence of oxygen. Tabata *et al.* (12) have reported that the activity of Al_2O_3 for NO reduction by methanol is enhanced considerably in the temperature region below 150°C by the addition of Sn.

Tin dioxide catalysts may exhibit different catalytic properties depending on the nature of the oxide carrier, since the metal oxide–support interaction affects both the redox properties and the dispersion of the active phase, the latter depending also on the tin content. In this study, we investigate the surface properties of tin dioxide catalysts supported on various acidic and basic supports (Al_2O_3, TiO_2, ZrO_2, SiO_2, and MgO).

At submonolayer coverage, the physicochemical properties of the surface species are strongly influenced by the oxide support to which they are coordinated, while at overmonolayer coverage the molecular structures of the guest oxide play an important role. In this paper we also report the influence of the tin loading on the catalytic properties of supported tin oxide catalysts, at submonolayer coverage and at tin content higher than the theoretical monolayer.

The number and the strength of Sn–O–Me bonds, specific to the oxide support, control the reducibility of the monolayer species and hence the reactivity of SnO_2 catalysts. It is

[1] To whom correspondence should be addressed. Fax: 33-4 72 44 53 99. E-mail: auroux@catalyse.univ-lyon1.fr.
[2] Deceased (1963–2000).

0021-9517/00 $35.00

generally accepted that the interfacial interaction between a solid substrate and a solid adsorbate greatly influences the surface structure and consequently the distribution of the various surface sites. We have therefore investigated the effect of these parameters on the surface reactivity and activity of tin oxide catalysts. The catalytic performances were tested in the selective reduction of nitrogen monoxide by ethene in the presence of excess oxygen.

To achieve the complete identification of the surface properties, a quantitative determination of the various surface sites is necessary, including the surface acid sites which are often involved in the catalytic activity of supported oxide materials. This knowledge can be obtained via adsorption calorimetry, using a gas with basic character, e.g., NH_3 (5, 13–15). Ammonia may act both as a Brønsted base by reaction with surface hydroxyl groups and as a Lewis base by reaction with electron acceptor surface sites.

To summarize, the aim of this study is to highlight the role played by the oxide carrier in the surface structures, acid–base properties, and reduction and oxygen readsorption patterns of tin oxide catalysts, providing relationships between reducibility, acidity, and reactivity.

TABLE 1

Composition and Properties of the SnO_2 Catalysts and Their Supports

Catalyst	Sn loading wt%	Sn loading mmol Sn · g^{-1}	BET surface $m^2 \cdot g^{-1}$	Surface coverage μmol Sn · m^{-2}
γ-Al_2O_3			110	
SnAl-3	3.1	0.261	108	2.42
SnAl-20	19.2	1.154	89	12.97
SiO_2			130	
SnSi-3	3.2	0.270	112	2.41
SnSi-20	21.7	1.828	96	19.04
TiO_2			103	
SnTi-3	3.4	0.286	90	3.18
SnTi-20	25.4	2.140	59	36.27
ZrO_2			90	
SnZr-3	3.4	0.286	78	3.67
SnZr-20	18.6	1.567	63	24.87
MgO			120	
SnMg-3	3.7	0.312	54	5.77
SnMg-20	23.5	1.980	25	79.20

II. MATERIALS AND METHODS

II.A. Preparation of Samples

The following oxide supports were used: γ-Al_2O_3 oxid C from Degussa, SiO_2 aerosil 130 from Degussa, TiO_2 anatase DT51 from Rhône Poulenc, ZrO_2 137 from Degussa, and MgO from Carlo Erba. The supported tin dioxide catalysts were prepared by the standard wet impregnation technique. The required amount of tin tetrachloride pentahydrate (Aldrich, 99.99% purity) was dissolved in distilled water and then slurried with each support.

The resulting mixture was evaporated to dryness and the powder further dried overnight at 100°C. This was followed by calcination in oxygen flow for 6 h at 150°C and then for 8 h at 500°C. Catalysts with loadings of about 3 wt% Sn (less than the monolayer) and 20 wt% Sn (above the monolayer) were prepared. Bulk SnO_2 was bought from BDH (purity > 99.9%, $S_{BET} = 9\ m^2/g$) and used as received.

II.B. Catalyst Characterization

Analysis of dissolved tin. The samples were subjected to elemental analysis in order to determine the amount of tin. This analysis was carried out by inductively coupled plasma (ICP) emission spectroscopy. Tin dioxide was dissolved in hydrochloric acid after melting at 1100°C with lithium tetraborate before analysis. The tin loadings are reported in Table 1, expressed both in weigth percent and in millimoles of Sn per gram.

X-ray diffraction measurements. The X-ray diffraction (XRD) technique was used to further confirm the crystallite size and the dispersion. The spectra of supports, supported tin dioxide and bulk tin dioxide catalysts, were obtained with a Philips diffractometer (PW 3710) using Cu $K\alpha$ radiation.

BET surface area measurements. After pretreatment at 400°C under vacuum, multipoint BET surface area measurements were performed using nitrogen as an adsorbate at −196°C. The naming of the samples according to the tin loadings as well as the values of surface areas are summarized in Table 1. The surface coverage calculated in micromoles of Sn per square meter of catalyst is also given.

Solid-state ^{119}Sn NMR spectra of the catalysts were obtained by using a Bruker spectrometer (DSX 400).

Mössbauer spectroscopy was used to control the valence states of tin in the samples.

Acidity measurements. In order to quantitatively determine the number and strength of the various acidic sites, chemisorption of ammonia was studied using the technique of adsorption calorimetry (5, 13–15).

A 100 mg portion of the support or catalyst was outgassed under vacuum for 6 h at 400°C prior to any measurement. The microcalorimetric studies were performed in a heat flow calorimeter (C80 from Setaram) at 150°C. The microcalorimeter was linked to a volumetric adsorption line, equipped with a Barocel capacitance manometer for pressure measurements. The differential heats of adsorption were measured as a function of coverage by repeatedly sending doses of gas onto the sample until an equilibrium pressure of about 66 Pa was reached. The sample was then evacuated for 1 h at the same temperature and a second adsorption was performed in order to allow

the determination of chemisorption uptakes. Ammonia was purified by successive freeze–thaw pumping cycles.

Temperature-programmed reduction (TPR)/oxidation (TPO). Temperature-programmed reduction (TPR) measurements were performed in a differential scanning calorimeter linked to a thermobalance (TG-DSC111 from Setaram), using quartz cells and a H_2/He mixture (80 vol% of H_2) flowing at 2.6 $L \cdot h^{-1}$. The symmetrical balance is arranged in a sealed enclosure connected to the calorimeter in the vertical position. The sample holders attached to the microbalance are placed in the microcalorimeter. The calorimetric measurements are performed with fluxmeters surrounding the tubes containing the sample holder but without physical contact. During the reduction, the gas flows in the two tubes were balanced out to minimize disturbances.

The reducing mixture was purified by passing it through a bed of activated molecular sieves and then through an oxysorb adsorbent to remove any water and oxygen. All experiments were carried out in the range 20–650°C with a heating rate of 3°C $\cdot$ min^{-1}. The mass change and heat flow signal were continuously recorded for data processing.

The sample weight was about 20 mg in order to avoid mass and heat transfer limitations.

After the reduction in flowing H_2/He mixture, the samples were cooled to room temperature and flushed at the same temperature for 15 min in the He carrier flow. Temperature-programmed oxidation (TPO) measurements were then performed with an O_2/He mixture (60 vol% O_2) flowing at 1.8 $L \cdot h^{-1}$.

Only the samples with high tin loading (20 wt% Sn) were studied by this method.

II.C. Catalytic Reaction

The catalytic reaction of NO reduction with ethene (NO–C_2H_4–O_2) was performed in a quartz tubular downflow microreactor (i.d. 5 mm) mounted in a tube furnace heated by a temperature controller (from Eurotherm) able to realize automatically programmed thermal sequences and isothermal steps. The reaction was studied at temperatures between 200 and 500°C; each examined temperature was maintained for 200 min and the overall test lasted 35 h. The reactant gases were special mixtures (2% NO/He and 1% C_2H_4/He) and pure O_2, supplied by Sapio (Italy), and were fed by independent mass flow controllers (Bronkhorst, Hi-Tec). The feed consisted of 0.5% of both NO and C_2H_4 and 9% O_2, with balance He. The total flow rate was 5.5 $L \cdot h^{-1}$, and 0.1 g of catalyst was used, which corresponded to a space velocity of 50,000 h^{-1}. The reaction products were analyzed by gas chromatography (Chrompack, CP-9000 equipped with TCD detector). A 60/80 Carboxen-1000 column (Supelchem) permitted the separation of O_2, N_2, CO, NO, CO_2, N_2O, and C_2H_4, operating as described in a previous paper (16). The catalysts were pretreated in He at 400°C for 4 h.

NO, which was fed together with O_2 and C_2H_4 in a He atmosphere, was partially converted to NO_2 in an oxygen atmosphere, leading to a mixture of NO_x. This mixture was converted to N_2 and N_2O, which are respectively the total and partial reduction products (N_2 and N_2O yields were evaluated on the basis of the NO fed). Conversion of C_2H_4 led to CO_2 as the main product and also CO (CO and CO_2 yields, evaluated on the basis of the C_2H_4 fed, equaled the C_2H_4 conversion at any temperature). Selectivity to the main product, N_2, was evaluated by means of the competitiveness factor (c.f., %), which is defined as the ratio between the amount of C_2H_4 consumed to reduce NO to N_2 and the total amount of C_2H_4 consumed (16, 17).

III. RESULTS

As can be seen from Table 1, the BET surface areas did not change appreciably upon impregnation of tin dioxide on silica and alumina, but were more affected on zirconia, titania, and magnesia, especially at high loading.

For the highly loaded sample on titania (SnTi-20), the mesoporosity of the support could be responsible for the decrease in surface area by pore plugging. The average pore diameter (≈13 nm for bare titania) did not decrease significantly (≈12 nm for SnTi-20) but the repartition of the pore volume as a function of the pore diameter has shown a dramatic plugging of the pores with diameter between 5 and 8 nm.

The decrease in surface area for the sample based on MgO (SnMg-20) can be interpreted by the formation of a mixed compound or a solid solution, as further confirmed by NMR.

The NMR spectra of the more loaded samples display only one peak centered around −601.5 ppm, except for SnMg-20 which shows a second peak at −481 ppm. This value of −601.5 ppm matches well with the isotropic resonance observed for pure SnO_2 (18). In view of the literature, it can be concluded that the Sn is present in an octahedral environment in all samples (18). For SiO_2, the peak is wider than for the other supports. This broadening is probably due to a lowering of local symmetry around Sn nuclei. The special pattern observed in the case of SnMg-20 implies that the octahedral Sn resonates, exhibiting another signal centered at −481 ppm. In the literature (19) the ^{119}Sn NMR of pure Mg_2SnO_4 exhibited an isotropic resonance at −483.5 ppm. The observed results have been attributed to Sn existing in an octahedral coordination but the SnO_6 octahedra are distorted in both lengths and bond angles. Our results are consistent with this literature report. However, the observed chemical shift is lower by about 2 ppm.

In the X-ray diffraction patterns (XRD), only the lines due to the supports were observed for the low-loading samples. However, in the case of the highly loaded samples, broad and weak lines due to SnO_2 also were observed.

There was no evidence of the presence of SnO or metallic Sn from XRD spectra.

The Mössbauer spectra of the SnO_2/Al_2O_3 samples exhibited a doublet with an isomer shift of 0.02 mm/s and a quadrupole splitting of ≈0.59 mm/s which can be assigned to SnO_2. Similarly for all samples, Mössbauer experiments showed no indication of the presence of either SnO or Sn metal.

III.A. TPR/TPO of Highly Loaded Tin Dioxide Catalysts

Figure 1 shows the temperature-programmed reduction profiles for supported SnO_2 catalysts, where the heat flow signal (mW) is plotted as a function of the increasing temperature (°C). The heat flow profiles of the highly loaded tin dioxide catalysts are given for a sample weight of 23 mg. One main endothermic peak with a more or less pronounced shoulder was obtained for all samples. This indicates that the oxidized tin is fixed on the supports in one or two types of species.

—SnAl-20 catalyst: The spectrum outlines a main reduction peak centered at 461°C with a shoulder at 530°C.

—SnSi-20 catalyst: A main reduction peak, asymmetric, with a maximum at 493°C, tightly convoluted with a large shoulder at 510°C.

—SnTi-20 catalyst: The TPR profile shows a main reduction peak with a maximum at 482°C and a shoulder at 415°C which could correspond to a partial reduction of the support.

—SnZr-20 catalyst: This system features a main reduction peak with a maximum at 429°C and quite a smaller one centered at 390°C.

—SnMg-20 catalyst: A main peak with a maximum at 447°C is found for this system, with a shoulder at 527°C.

The reduction peak locations are summarized in Table 2, together with the associated enthalpy variations and corresponding weight losses. For comparison the enthalpy change associated with the reaction $SnO_2 \rightarrow SnO$ is +296.9 kJ/mol (20).

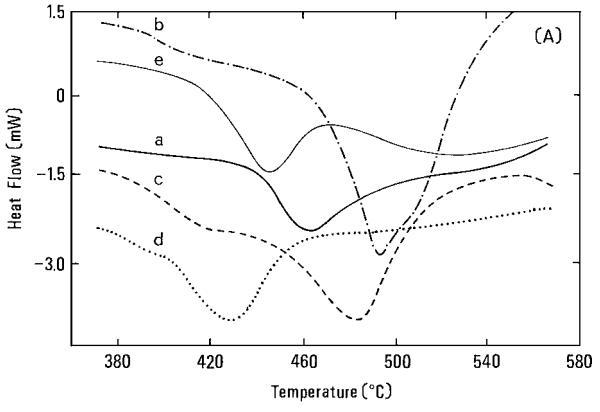

FIG. 1. TPR profiles (heat flow signal vs temperature) of the highly loaded supported tin dioxide samples: SnAl-20 (a), SnSi-20 (b), SnTi-20 (c), SnZr-20 (d), and SnMg-20 (e).

TABLE 2

TPR of SnO_2 Catalysts

Samples	$\Delta m/m$ (%)	Theoretical $\Delta m/m$ (%) $Sn^{IV}\rightarrow Sn^{II}$	Theoretical $\Delta m/m$ (%) $Sn^{IV}\rightarrow Sn^{0}$	ΔH (J/g), endo	T_{max} (°C)	Shoulder T (°C)
SnAl-20	1.6	2.58	5.17	+9	461	530
SnSi-20	5.0	2.93	5.85	+183	493	510
SnTi-20	5.0	3.42	6.84	+89	482	415
SnZr-20	2.9	2.50	5.01	+40	429	390
SnMg-20	1.7	3.17	6.33	+8	447	527

The heat flow profiles of the TPR of the bare oxide supports did not present any significant reduction peak under 600°C, except for TiO_2, the most reducible support, which showed a peak centered around 413°C.

The change of the tin valence during the reduction was calculated from the TG weight loss ($\Delta m/m$), as given in Table 2, column 2. This weight loss can be compared to the theoretical weight loss calculated from a valence change of 2 ($\Delta m/m$, Table 2 column 3). These results indicate that Sn^{II} is the main product of the reduction for samples SnAl-20, SnZr-20, and SnMg-20. In contrast, unsupported SnO_2 was reduced to metallic tin with a peak maximum at 520°C and a weight loss ($\Delta m/m$) of 21%, and no transition through SnO could be observed. Therefore, we must conclude that Sn^{II} is stabilized by the formation of a Sn^{II}–support surface complex. These results are in agreement with the literature (21).

However, we cannot exclude that a limited amount of reduction to metallic tin occurred on the supported samples, since a small endothermic peak was sometimes observed at 230–240°C (melting point of Sn) during reoxidation.

The higher the reduction temperature, the more stabilized the tin oxide should be. However, the stabilizing capacity of the support is sometimes exceeded, as was observed mainly with samples SnSi-20 and SnTi-20 on which part of the tin was reduced to the zero-valent state (Table 2).

The large shoulder which is observed between 510 and 530°C on some of the TPR profiles, and especially for SnSi-20, can be caused by the reduction of SnO to Sn. The formation of large SnO_2 crystallites on the silica surface behaving as bulklike SnO_2 explains a reduction temperature close to that of SnO_2.

The reducibility scale for $Sn^{IV} \rightarrow Sn^{II}$, based on the temperatures of the main peak maxima (T_{max}), is the following: $SnO_2/ZrO_2 > SnO_2/MgO > SnO_2/Al_2O_3 > SnO_2/TiO_2 > SnO_2/SiO_2$; the reducibility scale for $Sn^{IV} \rightarrow Sn^{0}$ is reversed. It will be shown below that this reducibility scale can also be rationalized in terms of acid–base properties of the carrier.

After TPR, the reduced samples were reoxidized by temperature-programmed oxidation (TPO) with a mixture

TABLE 3

TPO Experiments of Highly Loaded SnO_2 Catalysts

Sample	$\Delta m/m$ (%) 1st peak	$\Delta m/m$ (%) 2nd peak	ΔH (J/g), 1st peak (exo)	T_{max} (°C) 1st peak	T_{max} (°C) 2nd peak	Shoulder T (°C)
SnAl 20	1.6	—	−270	266	—	420
SnSi 20	2.4	—	−298	267	—	240
SnTi 20	1.3	5.0	−36	188	504	235
SnZr 20	1.2	0.3	−115	202	497	330
SnMg 20	1.45	3.4	−159	232	490	275

of 60% O_2 in He, and the oxygen consumption was monitored using the weight gain from the balance. The main purpose of TPO was to verify the stoichiometry observed for reduction.

The temperatures of the peak locations (main peak and shoulders) of the different samples are given in Table 3, together with oxygen uptake ($\Delta m/m$) and enthalpy variations. The heat flow profiles versus temperature for the previously reduced samples are given in Fig. 2. We can observe that for samples SnTi-20 and SnMg-20, the mass changes are superior to those obtained by reduction. It is likely a breakup of the mixed species on reduction and then increased oxidation, forming SnO_2 crystallites on TPO.

Bare oxide supports exhibited very low oxygen uptakes, quite negligible compared to those of supported SnO_2 catalysts. However, it is possible that the reactivity of the surface oxygen layer of the support governs the reducibility of tin oxide catalysts.

III.B. Acid–Base Properties

The results of adsorption calorimetry experiments performed with ammonia on the various samples and supports are given in Table 4. The residual amounts of ammonia adsorbed (V_{irr}), determined by the difference between the total adsorbed amount under an equilibrium pressure of 0.2 Torr (V_T) and the physisorbed amount (determined at the same pressure by readsorption after pumping), are given together with the integral heats of adsorption (total heat evolved under 0.2 Torr of equilibrium pressure). We can consider that V_{irr} measures the amount of strongly adsorbed ammonia on the surface at 150°C.

The results show that the SnSi and SnMg materials display a greater number of strong acid sites than the respective supports, while in contrast the SnTi samples show a decrease in the number of acid sites, especially at high loading. The total acidity of zirconia is nearly unaffected by 3 wt% of Sn, and is decreased in the presence of 20 wt% of Sn. On alumina a peculiar behavior was observed, with an increase of acidity in the presence of only 3 wt% of Sn, while the acidity is again close to that of the support when the loading reaches 20 wt% of Sn.

Figure 3 represents the site-energy distributions, which provide information on the strength and distribution of the acid sites of the various samples by plotting the number of sites within a given interval of evolved heat.

On alumina (Fig. 3a), it is clear that the number of weak acid sites ($50 < Q < 100$ kJ · mol^{-1}) does not vary with the tin loading while the numbers of strong ($Q > 150$ kJ · mol^{-1}) and medium acid sites ($100 < Q < 150$ kJ · mol^{-1}) are much more affected. Adding a low amount of tin dioxide to alumina decreases the number of strong sites and increases the number of medium sites, while a high SnO_2 loading creates

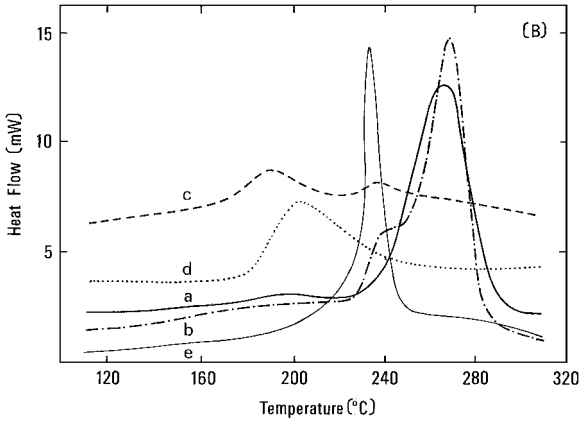

FIG. 2. TPO profiles (heat flow signal vs temperature) of the highly loaded supported tin dioxide samples: SnAl-20 (a), SnSi-20 (b), SnTi-20 (c), SnZr-20 (d), and SnMg-20 (e).

TABLE 4

Acidity Measurements

Samples	Q_{init}[a] (kJ/mol)	V_T[b] (μmol/g)	V_{in}[c] (μmol/g)	Q_{int}[d] (J/g)
γ-Al_2O_3	187	188.2	105.6	22.5
SnAl-3	187	216.5	123.1	25.6
SnAl-20	177	187.5	104.8	22.3
SiO_2	68	26.2	10.7	0.7
SnSi-3	168	61.0	28.8	3.5
SnSi-20	171	54.5	30.3	3.3
TiO_2	164	282.2	165.0	34.0
SnTi-3	166	259.9	159.0	31.4
SnTi-20	167	185.9	103.5	20.6
ZrO_2	184	234.3	119.4	27.7
SnZr-3	168	233.4	134.7	28.9
SnZr-20	174	193.3	109.3	21.9
MgO	61	27.7	11.2	0.6
SnMg-3	150	88.5	27.2	8.4
SnMg-20	114	90.2	34.5	6.7

[a] Initial heat of NH_3 adsorption at zero coverage.

[b] Total volume of NH_3 adsorbed under an equilibrium pressure of 0.2 Torr.

[c] NH_3 chemisorbed volume determined by difference between V_T and the readsorbed volume after pumping.

[d] Integral heat of adsorption corresponding to the same coverage as V_T.

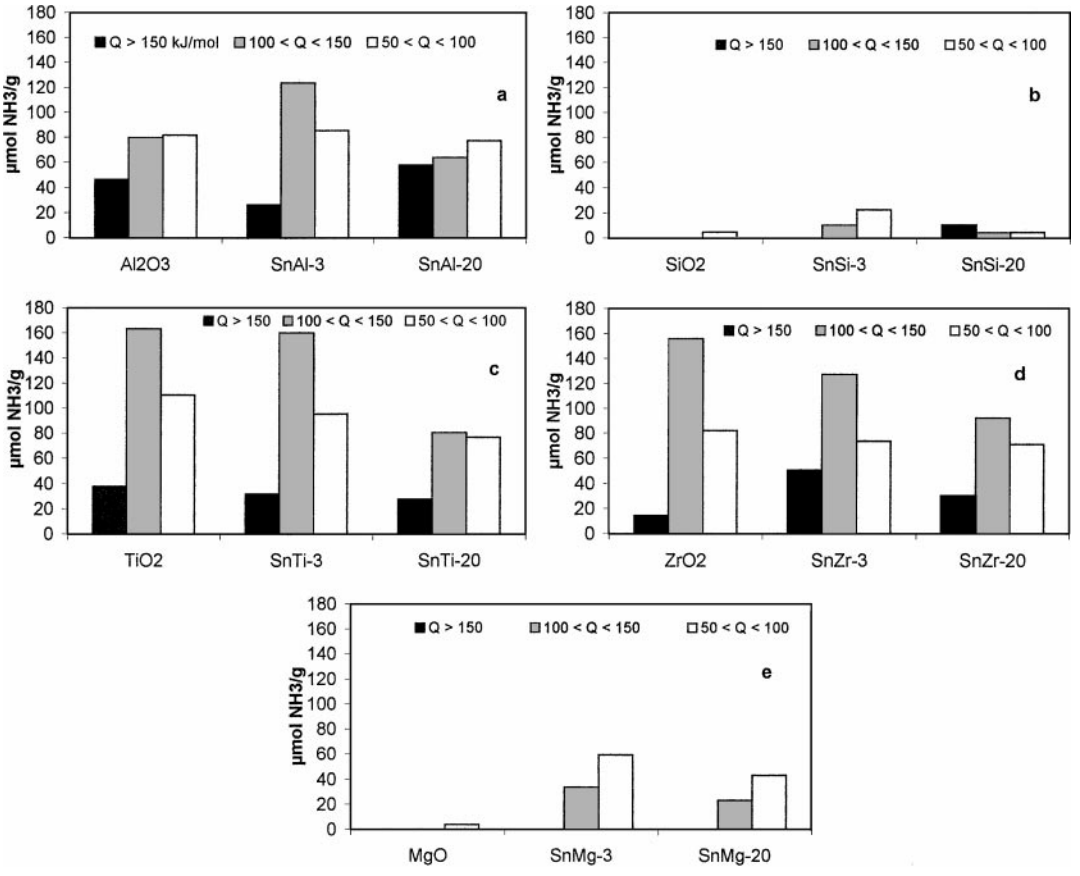

FIG. 3. Site-energy distributions (number of acid sites of a given strength) of the various samples.

some strong sites but decreases the number of medium sites. On the SiO_2 support (Fig. 3b) the addition of 3 wt% Sn enhances considerably the number of weak sites, and new acid sites are formed in the range of differential heat between 100 and 150 kJ · mol^{-1}. At high loading (20 wt% Sn), strong sites are created. However, the adsorbed ammonia volume remains the lowest of the series of samples.

The series of materials using titania (Fig. 3c) and zirconia (Fig. 3d) as supports are similar in their behavior. The presence of SnO_2 on these supports does not create much acidity (a few strong sites are created on ZrO_2 at low loading), and even at high loading we observe a decrease in acidity in the whole range of differential heat between 150 and 50 kJ · mol^{-1}. The most dramatic change of the overall acidity by adding SnO_2 was observed for MgO-based samples (Fig. 3e), despite the important reduction of the surface area. A small amount of tin dioxide increases drastically the number of medium and weak acid sites, while a high loading decreases the number of these sites. This can be explained by a poor dispersion of SnO_2 at the surface of the high-loading sample, and also possibly by a structural transformation to a mixed oxide.

The effect of tin on the acid–base properties of γ-Al_2O_3 has been studied by Shen *et al.* (5) by microcalorimetric measurements of the heats of ammonia adsorption. They found that the addition of SnO_2 to γ-Al_2O_3 decreases the number of strong acid sites ($Q > 140$ kJ/mol) and increases the number of weaker sites ($110 < Q < 130$ kJ/mol). These results are in agreement with those of our previous studies (22–24).

The acid–base properties of Al_2O_3–SnO_2 systems have also been studied by Kirszensztejn *et al.* (25, 26), using the decomposition of isopropanol and the conversion of cumene to measure the changes in the acidic–basic catalytic sites. They found that the number of strong Lewis acid sites is diminished by the addition of Sn and that strong Brønsted acid sites do not appear. However, they did not exclude the formation of weak Brønsted acid sites.

III.C. Selective Reduction of NO by C_2H_4

The Sn-based catalysts prepared on different supports were evaluated in the NO–C_2H_4–O_2 reaction according to their activities and selectivities (expressed in terms of the competitiveness factor). Figure 4 shows a typical reaction profile obtained for the SnZr-3 catalyst as a function of reaction temperature, using 0.5% of both NO and C_2H_4 and 9% O_2 at 50,000 h^{-1} (GHSV) of space velocity. Significant

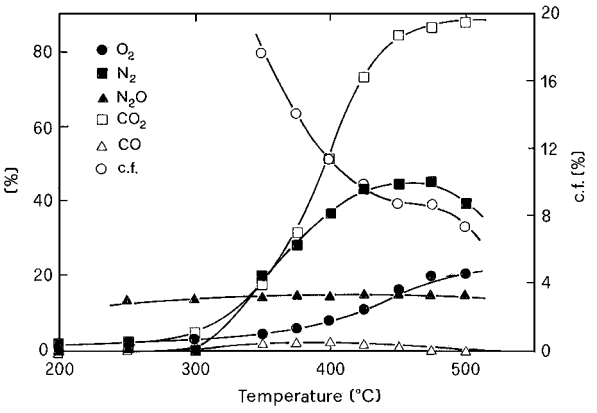

FIG. 4. $NO–C_2H_4–O_2$ reaction profile (feed, 0.5% NO, 0.5% C_2H_4, and 9% O_2): yields (%) to N_2, NO_2 and to CO_2, CO and conversion (%) of O_2 as a function of reaction temperature for the SnZr-3 catalyst at 50,000 h^{-1} (GHSV). The secondary axis shows the competitiveness factor (c.f.,%).

conversion of NO to N_2 as well as of C_2H_4 to CO_2 was detected above 350°C. Plotting the N_2 yield versus temperature led to a volcano-shaped curve, as usually observed for most lean NO_x catalysts (27, 28). The CO_2 yield increased sharply up to 500°C but did not reach a concentration relevant to complete conversion of C_2H_4. Oxygen conversion became appreciable around 375–400°C, indicating that C_2H_4 combustion took place actively in this temperature domain. This behavior affected the selectivity of the catalyst, and a remarkable decrease of the competitiveness factor could be observed, from about 18% down to 9% at 350 and 450°C, respectively. By-products of partial reduction, N_2O, and oxidation, CO, were observed too; the amount of N_2O remained almost constant at any time and temperature of reaction. Analogous reaction profiles were observed for the Sn catalysts on the other supports (Al_2O_3, TiO_2, and SiO_2). Among the catalysts, significant differences in the yields of the various products and in the temperatures of onset of the NO reduction were observed. The most active catalysts were those prepared on ZrO_2 and Al_2O_3. Quantitative conversion of the hydrocarbon was not observed in any case. The Sn catalyst based on MgO produced no N_2 and only very low amounts of CO_2.

Figures 5a–5e compare the N_2 and CO_2 yields for the $NO–C_2H_4–O_2$ reaction over the Sn-based catalysts at low (3 wt%) and high (20 wt%) loading on each support, under the same reactant concentrations and space velocity as mentioned above. The catalysts prepared on Al_2O_3, SiO_2, TiO_2, and ZrO_2 led to NO conversions to N_2 in the range 30–50%. A clear effect on the $NO–C_2H_4–O_2$ activity of the amount of Sn deposited was not observed. In fact, similar trends were observed in the curves of the N_2 and CO_2 yields as a function of temperature on the low and high Sn loading catalysts on each support. In some cases (SiO_2 and ZrO_2 supports), the high (20 wt%) Sn loading catalysts were more active than the corresponding less loaded (3 wt%) ones, while opposite trends were observed over Al_2O_3 and TiO_2 supports. Two different activity scales based on the performance for NO reduction to N_2 and for C_2H_4 oxidation to CO_2 could be compiled: SnZr > SnAl > SnTi ≫ SnSi ≫ SnMg and SnSi > SnZr > SnTi > SnAl ≫ SnMg, respectively.

Concerning selectivity, the N_2O yields were in the 10–15% range, and independent of temperature over the low-loading Sn-based catalysts, while N_2O was absent (SnAl-20 and SnTi-20) or present only in a limited temperature interval (SnSi-20 and SnZr-20) over the high-loading Sn catalysts. For CO formation, higher yields were observed over the less loaded catalysts. The catalysts based on Al_2O_3 and TiO_2 gave rise to higher amounts of CO (ca. 12%) than those based on ZrO_2 (ca. 1–2%).

The competitiveness factor (c.f.) indicates the efficiency of the catalyst for NO_x reduction. It can be regarded as a practical parameter to evaluate selectivity to N_2 formation, as the $NO–C_2H_4–O_2$ reaction can be viewed as a process in which two oxidants, NO_x and O_2, compete for a limited available amount of hydrocarbon reductant (16). Figure 6 shows the trend of c.f. (%) as a function of the reaction temperature. As expected, a decrease of c.f. with temperature is observed in all cases. As the temperature increases, the combustion of C_2H_4 by O_2 becomes the dominant reaction in comparison with C_2H_4 oxidation by NO_x. The very high values of c.f. at low temperatures (<400°C), which are the highest ever reported so far, in agreement with previous observations by Kung *et al.* (9), are especially worthy of attention. At higher temperatures, we observed sustained O_2 conversion and nearly complete conversion of C_2H_4 to CO_2; c.f. values ranged from 5 to 10%, indicating that the oxidation of C_2H_4 by NO_x was still occurring. Among SnO_2 catalysts, those prepared on Al_2O_3 were the most selective at any temperature.

Table 5 summarizes the activity of the Sn-based catalysts in terms of temperature of onset of NO conversion to N_2

TABLE 5

Summary of the Activity and Selectivity in the $NO–C_2H_4–O_2$ Reaction over the SnO_2 Catalysts on Different Supports

Catalyst	T_{on}[a] (°C)	T_{max}[a] (°C)	10^3 Specific activity[b] (s^{-1})	c.f.[b] (%)
SnAl-3	350	475	4.86	11.1
SnAl-20	375	500	0.716	8.1
SnSi-3	385	475	3.14	6.2
SnSi-20	365	450	0.578	6.2
SnTi-3	325	475	3.67	8.1
SnTi-20	350	475	0.488	7.2
SnZr-3	345	475	4.87	8.6
SnZr-20	345	425	0.99	9.5

[a] T_{on} corresponds to 10–15% N_2 yield; T_{max} corresponds to maximum observed N_2 yield.

[b] Specific activity and c.f. calculated at T_{max}.

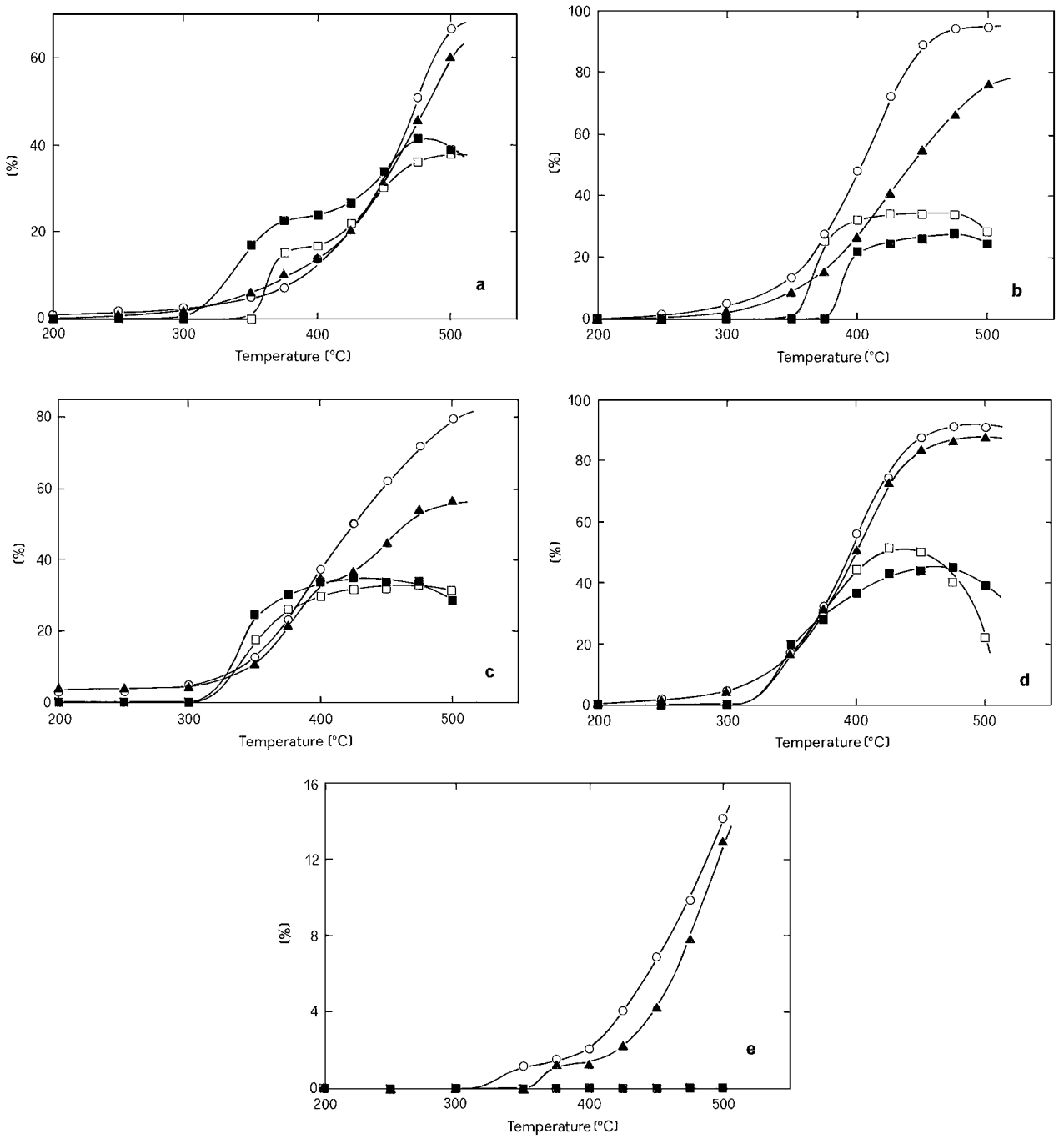

FIG. 5. (a) NO conversion to N_2 and C_2H_4 conversion to CO_2 in the NO–C_2H_4–O_2 reaction as a function of reaction temperature for the SnAl-3 and SnAl-20 catalysts. SnAl-3: filled square (N_2) and filled triangle (CO_2). SnAl-20: open square (N_2) and open circle (CO_2). (b) NO conversion to N_2 and C_2H_4 conversion to CO_2 in the NO–C_2H_4–O_2 reaction as a function of reaction temperature for the SnSi-3 and SnSi-20 catalysts. SnSi-3: filled square (N_2) and filled triangle (CO_2). SnSi-20: open square (N_2) and open circle (CO_2). (c) NO conversion to N_2 and C_2H_4 conversion to CO_2 in the NO–C_2H_4–O_2 reaction as a function of reaction temperature for the SnTi-3 and SnTi-20 catalysts. SnTi-3: filled square (N_2) and filled triangle (CO_2). SnTi-20: open square (N_2) and open circle (CO_2). (d) NO conversion to N_2 and C_2H_4 conversion to CO_2 in the NO–C_2H_4–O_2 reaction as a function of reaction temperature for the SnZr–3 and SnZr-20 catalysts. SnZr-3: filled square (N_2) and filled triangle (CO_2). SnZr-20: open square (N_2) and open circle (CO_2). (e) NO conversion to N_2 and C_2H_4 conversion to CO_2 in the NO–C_2H_4–O_2 reaction as a function of reaction temperature for the SnMg-3 and SnMg-20 catalysts. SnMg-3: filled square (N_2) and filled triangle (CO_2). SnMg-20: open square (N_2) and open circle (CO_2).

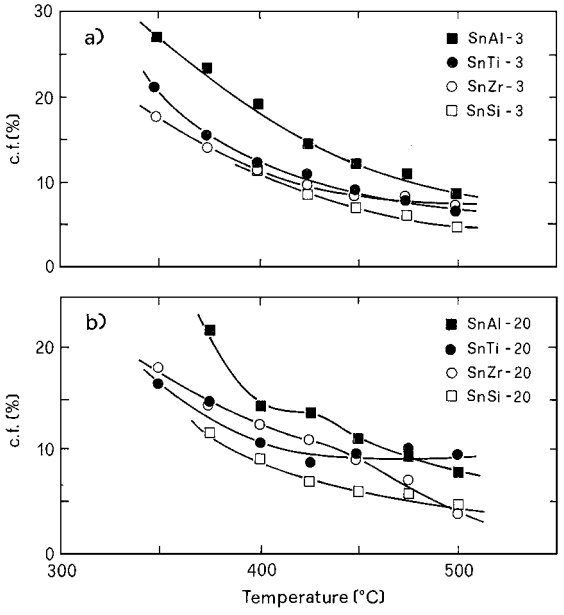

FIG. 6. Trend of the competitiveness factor (c.f.,%) versus the reaction temperature in the NO–C_2H_4–O_2 reaction for the Sn-based catalysts on the different supports: (a) low Sn catalysts (3 wt%) and (b) high Sn catalysts (20 wt%).

(T_{on}), temperature of maximum NO conversion (T_{max}), integral rate to N_2 formation at T_{max} (i.e., specific activity, calculated as the amount of N_2 formed per mole of Sn per second), and selectivity, expressed in terms of competitiveness factor, at T_{max}. The temperatures of maximum activity for NO conversion to N_2 were in the 425–500°C range, independent of the support and of the Sn loading. Integral rates of N_2 formation were higher on the low Sn loading catalysts ($3–5 \times 10^{-3}\,s^{-1}$) than on the high Sn ones ($0.5–1 \times 10^{-3}\,s^{-1}$). The activity per mole of Sn decreased with increasing Sn loading because of decreasing SnO_2 dispersion.

IV. DISCUSSION

The present study reports an excellent activity of some supported tin dioxide catalysts such as Sn/Zr and Sn/Al samples for the selective reduction of NO_x with hydrocarbons in oxidizing atmospheres. Since it has been speculated that the acidity of zeolites is responsible for their performance in selective reduction, the relationship between the activity and acidity of the catalysts has to be discussed (3).

As variations of acid–base properties with catalyst composition were observed, we can ask if the role played by surface acidic and basic sites of oxides in determining activity and selectivity is as important in the case of the SCR of NO by hydrocarbons as in other reactions.

The trends observed in acid–base properties clearly correlate with those for surface tin composition, as acid sites are related to surface tin cations. The acidic adsorption centers may consist of electrophilic oxygen associated with Sn^{4+} cations (29).

An analysis to find a linear correlation between the acidity values and the catalytic activity failed to provide a clear answer, although the results indicate that a certain sizeable amount of acidity is needed in order to achieve high c.f. values. The activity appears to increase with a moderate acidity.

The adsorption calorimetry results, shown in Table 4, indicate that new acid sites are formed by supporting 3 wt% Sn on SiO_2, MgO, and Al_2O_3. This increase of acidity can be ascribed to the strong interaction of highly dispersed SnO_2 with weakly or moderately acidic supports.

On the most acidic supports (TiO_2, ZrO_2) the deposited SnO_2 is comparatively less acidic than the support and does not generate any additional acidity.

In the case of highly loaded samples (20 wt%), no additional increase of acidity is observed, and even a decrease in acidity is observed compared to the low-loading samples. SnO_2 particles are too thick for new acid sites to be formed on the support. The moderate acid strength of the different catalysts with high SnO_2 content may be ascribed to weak interaction or, in other words, to large SnO_2 particles.

It is worth noting that the moderate acid strength of all catalysts may suppress coke deposition. Thus, the relatively small amount of very strong acid sites resulted in high selectivity of SnO_2-based catalysts.

The impact of the support on the redox potential of tin dioxide (as evidenced from TPR/TPO experiments) can be used to help understand the observed differences in activity and selectivity of the highly loaded samples.

It is evident that the reduction/oxidation behavior of these catalysts depends on the nature of the species on the support. In addition, the partial pressure of H_2 used in the experiments also affects the degree of reduction.

It is expected that, as the tin dioxide species become more bulklike, i.e., as the particle size increases with an increase in loading, tin dioxide becomes more difficult to reduce, due to bulk diffusion limitations resulting in a shift of the TPR peaks to higher temperatures.

Figure 7 represents the competitiveness factor as reported in Table 5 versus the temperature of the reduction peak maximum for the samples with a high tin dioxide loading. As can be seen, a nearly linear correlation is obtained. This correlation means that an easy and reversible reduction of Sn^{IV} to Sn^{II} (good dispersion, small particles) is favorable to the reaction, while the direct passage from Sn^{IV} to Sn^0 (bad dispersion, large SnO_2 particles) has a negative influence.

At low SnO_2 loading, alumina, titania, and zirconia, which are acidic supports, behave similarly, with a strong interaction effect between SnO_2 and the support creating SnO_2 species well suited to the reaction of NO reduction by C_2H_4 in the presence of O_2. On basic MgO and weakly acidic SiO_2, the resulting species are less reactive.

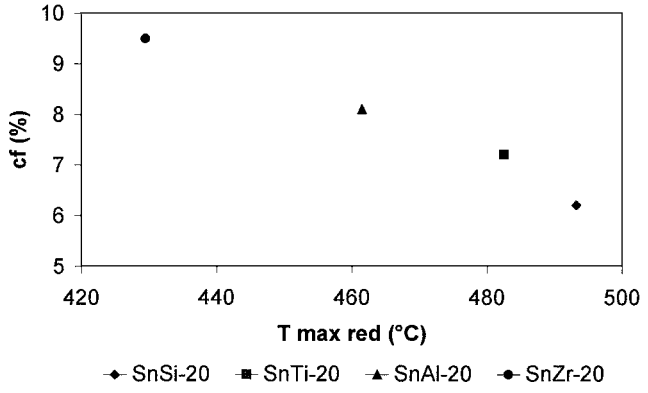

FIG. 7. Competitiveness factor (%) as a function of the temperature of the reduction peak maxima (°C) for highly loaded tin dioxide samples.

It can be seen that the amount of SnO_2 is not the most important factor, as the catalytic activity is not deeply affected by an increase in loading. The activity is only slightly decreased, whether SnO_2 is present as large crystallites or well-dispersed.

The most active sites seem to correspond to well-dispersed SnO_2 that can be reduced to Sn^{II} rather than Sn^0. It is sufficient for the surface to be covered by a minimal amount of SnO_2 in order to achieve optimal catalytic performance. Additional loading affects the catalytic activity only slightly, and no sharp drop in activity is observed, unlike what happens in the case of copper catalysts, where the agglomeration of CuO leads to complete inactivation of the catalyst (25).

SnO_2-based catalysts resemble those that contain nonreducible cations, such as Ga_2O_3 catalysts, although in several aspects their behavior is similar to that of catalysts composed by reducible cations, such as Cu–ZSM-5. Therefore, SnO_2 catalysts have been recognized as a unique kind of lean NO_x catalysts (8, 30). One of their peculiar characteristics is their poor ability to activate hydrocarbons. The support plays an important role by dispersing the active phase, thus increasing the number of active centers. In this perspective, supports that react with metal oxides by forming solid compounds, as in the case of SnO_2 on MgO, are not expected to be active in the lean NO_x process.

CONCLUSION

On supported metal oxide catalysts, the nature of the surface species depends on the type and strength of the acidity available on the surface of the support, and the level of dispersion of the active metal has been found to depend on the nature of the bonding between the metal species and the available centers of the support. So, the promotive effect of SnO_2 is due to the interaction of Sn with the support.

The superior activity and selectivity of the low-loading samples may be the result of the high dispersion of the active metal and the stabilization of the dispersed phase by the host oxide. The acidity of the support plays a major role in stabilizing the active phase but we suspect that the redox character of the catalysts is the main factor that determines catalytic activity. However, further studies will be necessary in order to identify the true active centers of the catalysts and the reaction mechanism. For this purpose, an in-depth investigation of the tin loading controlling surface species and relation with activity is in progress.

ACKNOWLEDGMENTS

The authors thank Dr. F. Lefebvre (COMS, CPE Lyon, France) for providing NMR spectra and Dr. B. Bonnetot (LPCM, Université Claude Bernard, Lyon I, France) for providing XRD spectra. Financial support by the Commission of the European Union under Grant ERBIC15CT980515 is gratefully acknowledged.

REFERENCES

1. Shimokawake, M., Ohi, A., and Takezawa, N., *React. Kinet. Catal. Lett.* **52**, 393 (1994).
2. Hamada, H., *Catal. Today* **22**, 21 (1994).
3. Kintaichi, Y., Hamada, H., Tabata, M., Sasaki, M., and Ito, T., *Catal. Lett.* **6**, 239 (1990).
4. Jimenez, V. M., Mejias, J. A., Espinos, J. P., and Gonzalez-Elipe, A. R., *Surf. Sci.* **366**, 545 (1996).
5. Shen, J., Cortright, R. D., Chen, Y., and Dumesic, J. A., *Catal. Lett.* **26**, 247 (1994).
6. Tagawa, T., Kataoka, S., Hattori, T., and Murukami, Y., *Appl. Catal.* **4**, 1 (1982).
7. Hattori, T., Itoh, S., Tagawa, T., and Murakami, Y., *in* "Preparation of Catalysts IV" (B. Delmon, et al., Eds.), Studies in Surface Science, p. 113, Elsevier, Amsterdam, 1987.
8. Park, P. W., Kung, H. H., Kim, D.-W., and Kung, M. C., *J. Catal.* **184**, 440 (1999).
9. Kung, M. C., Park, P. W., Kim, D.-W., and Kung, H. H., *J. Catal.* **181**, 1 (1999).
10. Miyadera, T., and Yoshida, K., *Chem. Lett.* 1483 (1993).
11. Teraoka, Y., Harada, T., Iwasaki, T., Ikeda, T., and Kagawa, S., *Chem. Lett.* 773 (1993).
12. Tabata, M., Hamada, H., Kintaichi, Y., Sasaki, M., and Ito, T., *Catal. Lett.* **25**, 55 (1994).
13. Auroux, A., *Topics Catal.* **4**, 71 (1997).
14. Gervasini, A., and Auroux, A., *J. Phys. Chem.* **97**, 2628 (1993).
15. Auroux, A., Fenyvesi, J., and Gervasini, A., *Langmuir* **12**, 5356 (1996).
16. Gervasini, A., Carniti, P., and Ragaini, V., *Appl. Catal. B* **22**, 201 (1999).
17. Bethke, K. A., Kung, M. C., Yang, B., Shah, M., Alt, D., Li, C., and Kung, H. H., *Catal. Today* **26**, 169 (1995).
18. Velu, S., Suzuki, K., Okazaki, M., Osaki, T., Tomura, S., and Ohashi, F., *Chem. Mater.* **11**, 2163 (1999).
19. Clayden, N. J., Dobson, C. M., and Fern, A., *J. Chem. Soc., Dalton Trans.* 843 (1989).
20. Cox, J. D., Wagman, D. D., and Medvedev, V. A., "Codata key values for thermodynamics," p. 1, Hemisphere, New York, 1984.
21. Lieske, H., and Völter, J., *J. Catal.* **90**, 96 (1984).

22. Sprinceana, D., Caldararu, M., Ionescu, N. I., and Auroux, A., *J. Therm. Anal. Calorim.* **56**, 109 (1999).
23. Gergely, B., and Auroux, A., *Res. Chem. Intermed.* **25**, 13 (1999).
24. Gergely, B., Redey, A., Guimon, C., Gervasini, A., and Auroux, A., *J. Therm. Anal. Calorim.* **56**, 1233 (1999).
25. Kirszensztejn, P., Przystajko, W., and Bell, T. N., *Catal. Lett.* **18**, 391 (1993).
26. Sheng, T. C., Kirszensztejn, P., Bell, T. N., and Gay, I. D., *Catal. Lett.* **23**, 119 (1994).
27. Gervasini, A., Picciau, C., and Auroux, A., *Microporous Mesoporous Mater.* **35–36**, 457 (2000).
28. Okazaki, N., Shiina, Y., Itoh, H., Tada, A., and Iwamoto, M., *Catal. Lett.* **49**, 169 (1997).
29. McAtcer, J. C., *J. Chem. Soc., Faraday Trans. 1* **75**, 2762 (1979).
30. Kung, M. C., and Kung, H. H., *Topics Catal.* **10**, 21 (2000).